# Section I

# Measurements

# 1

# *Comparison of Biological Scale Resolution from CTD and Microstructure Measurements*

**Fabian Wolk, Laurent Seuront, Hidekatsu Yamazaki, and Sophie Leterme**

**CONTENTS**



## 1.1 Introduction

The existence of small-scale (<1 m) planktonic structures and their importance to the dynamics of the aquatic ecosystem are now widely acknowledged in the oceanographic and limnology community (e.g., Hanson and Donaghay, 1998; Holliday et al., 1998; Jaffe et al., 1998; Franks and Jaffe, 2001). Despite recent advances in experimental technology (Mitchell and Fuhrman, 1989; Donaghay et al., 1992; Desiderio et al., 1993), most field work is conducted using conventional sampling methods (such as Niskin bottles or *in situ* fluorometers mounted on CTD cages), which do not resolve the small-scale biological structures.

Recently, the study of the intermittent variability of biological processes in aquatic ecosystems has benefited from the development of small-scale monitoring systems (Hanson and Donaghay, 1998; Holliday et al., 1998; Jaffe et al., 1998; Franks and Jaffe, 2001), and novel theoretical approaches to characterize intermittent patterns (Pascual et al., 1995; Strutton et al., 1996, 1997; Seuront et al., 1999). These techniques confirm the notion that any advances in understanding the response of fine-scale and microscale biological structures to physical forcing require simultaneous measurements of both physical and biological parameters over a congruent range of spatial scales. With the exception of a few studies (Donaghay et al., 1992; Desiderio et al., 1993; Cowles et al., 1998;Yamazaki et al., 2002a) previous small-scale biological observations have lacked concomitant measurements of physical variables. Such information is, however, of crucial importance because physical processes at these scales (e.g., shear instabilities, convective overturns, salt fingering, etc.) lead to intermittent vertical mixing and the redistribution of biomass. Such correlated measurements are particularly important in highly dissipative environments, such as tidally mixed coastal waters, frontal structures, or turbulent patches in the seasonal

0-8493-1344-9/04/$0.00+$1.50

thermocline, where the space and time variability of physical and biological processes and the resultant biophysical interactions are very high (Yamazaki and Osborn, 1988; Yamazaki et al., 2002b).

To understand the response of phytoplankton cells to physical forcing, it is necessary to accomplish the following:

1. Describe the vertical structure of the sampled water column in terms of physical parameters
2. Identify the spatial patterns of concurrently sampled *in vivo* fluorescence (a proxy of phytoplankton biomass)
3. Investigate its potential fine and microscale relationships with the surrounding physical environment.

In this context, the purpose of this chapter is to stress the importance of fine-scale sampling methods in aquatic ecology, and to demonstrate how the use of adequate high-resolution experimental equipment, coupled with novel statistical tools for processing and analyzing the data, can increase our understanding of the structures of the aquatic ecosystem. It is shown that the chlorophyll *a* concentration inside a single Niskin bottle is far from homogeneous; concentration values can vary more than the annual distribution range from the same sampling area. Data from a high-resolution fluorometer deployed in a lake and a well-mixed tidal channel corroborate the high degree of small-scale variance found in the Niskin bottles. This small-scale structure is often overlooked in standard CTD sampling methods. Finally, it is shown that new experimental equipment and appropriate higher-order statistical tools make it possible to condense the high-resolution data and effectively characterize the experimental results. In Section 1.2.1, the current understanding of aquatic ecosystem structures and functions is outlined. An example of field samples taken from Niskin bottles demonstrates the impact of the sampling strategy on the observed microscale distribution of phytoplankton biomass (Section l.2.2). A direct comparison of field data from a recently developed high-resolution bio-optical sensor and a conventional field fluorometer illustrates how inappropriate equipment can lead to a distorted representation of the biological structures in the water column. The results of the comparison are described in Section l.3.

## 1.2 Microscale Structure in Aquatic Ecosystems: Perspectives

Accurate characterization of phytoplankton distributions, as well as their sources and scales of variability, is important for a variety of applications; e.g., basic studies of primary production (Platt et al., 1989; Seuront et al., 1999), issues related to the role of particle aggregates in the vertical flux of organic matter (Jackson and Burd, 1998), modeling the effects of thin layer reflectance on remote sensing (Petrenko et al., 1998; Zaneveld and Pegau, 1998), and studying the effects of light absorption by phytoplankton and particulate material (Sosik and Mitchell, 1995).

It has been recognized for more than two decades that physical and biological structures, identified in terms of spatial patchiness, temporal cycles, or disturbances, are a key feature of aquatic ecosystems (Denman and Powell, 1984; Mackas et al., 1985). The geometry of such structures and their effect on the aquatic ecosystem depends on both their magnitude and their spatial and temporal scales.

### 1.2.1 Aquatic Ecosystem Functioning

Biophysical interactions affect the ecosystem in a subtle manner because the effects depend on the coupling between physical scales of patchiness and biologically significant scales, such as generation time or ambits. The effects of a particular scale of patchiness may vary for different types of organisms with different characteristic biological scales. Biophysical disturbances, for example, have been proposed as a potential mechanism for maintenance of diversity under conditions where competitive exclusion should otherwise lead to lower diversity (Hutchinson, 1961; Scheffer, 1995; Siegel, 1998; Seuront et al., 2002; Seuront and Spilmont, 2002). The scales of disturbance that are necessary to allow coexistence

in this manner for phytoplankton (with generation times of days and ambits of decameters or less) may differ from that of macrozooplankton (with generation times of weeks to months and ambits over this time of at least tens of kilometers). The outcome of other interactions, such as feeding, predation, or migration of zooplankton, may also depend on the interrelation between scales of physical structure and the biological and/or ecological scale on which the process takes place.

The ambit of planktonic organisms depends on both their movements in the water and the motion of the water. The planktonic patchiness in the ocean depends highly on mixing and stirring, as well as the size, intensity, and persistence of patches. Hence, a description of the relative patchiness of physical and biological processes, together with the extent of their spatial and temporal scales, as well as a comparison of such patterns with biologically important scales, may lead to a better understanding of the effect of biophysical patchiness on aquatic ecosystem structure and function. For example, observations of zooplankton swimming behavior have demonstrated that swimming abilities of zooplankton can in most aquatic environments overcome the effects of the root-mean-square turbulent velocities (Schmitt and Seuront, 2001; Chapter 22, this volume), which confirms previous hypotheses based on literature survey (Yamazaki and Squires, 1996; Seuront, 2001). This suggests that the effects of turbulence on planktonic contact rates could be less important than previously thought.

The key processes of the structure and function of the aquatic ecosystem take place at the microscale (i.e., at scales where molecular viscosity and diffusion become important). A salient issue in aquatic ecology is, therefore, the development of instrumentation and numerical tools to identify and characterize patchiness in both physical parameters (e.g., temperature, salinity, and shear) and phytoplankton distribution. Recent numerical investigations focus on (1) the effects of turbulence intermittency on predator–prey encounter rates, physical coagulation rates, and the flux of nutrient toward nonmotile phytoplankton cells; and (2) the effect of phytoplankton patchiness on predator–prey encounter rates via predator behavioral adaptation (Seuront, 2001; Seuront et al., 2001). To improve our understanding of aquatic ecosystem structure and function we must, therefore, integrate the microscale structure of physical and biological parameters to estimate major biochemical fluxes.

### 1.2.2 Impact of the Sampling Process

Conventional sampling approaches implicitly assume that biological processes are in a steady state. Measurements from different cruises or stations are compared assuming that spatial and temporal changes are minimal. However, patchiness, spatial gradients (e.g., fronts), temporal cycles (e.g., tidal, seasonal, or interannual), and both spatial and temporal microscale patchiness elevate the uncertainty of such comparisons. Generally speaking, a description of patchiness in different scales may help design effective sampling schemes. More specifically, if microscale patchiness exists, an appropriate sampling device is required to investigate the nature of patchiness.

As an example, we investigated the effect of patchiness in the sampled water in a Niskin bottle (Figure 1.1A). It is standard experimental practice to draw a number of subsamples from the Niskin bottle, according to the number of studied parameters. The unused remainder inside the Niskin bottle is often dumped. For example, if information is needed of phytoplankton biomass and production, particulate organic material (POM), dissolved organic material (DOM), and nutrient concentration, the sampling unit will be divided into five uniform subsamples (as illustrated in Figure 1.1B). Each subsample is regarded as representative of the entire bottle contents, analyzed separately, and then correlated with the other parameters to infer causality between them. However, such a sampling scheme assumes spatial homogeneity within the original sampling bottle, and thus spatial homogeneity between the subsamples. This is, however, deeply questioned, at least in the case of phytoplankton populations, where the centimeter-scale patchiness of phytoplankton has been clearly demonstrated in several studies (Yamazaki et al., 2002a; present study). Moreover, based on recent results obtained on bacteria (Seymour et al., 2000) and nutrient (Seuront et al., 2002), it is reasonable to assume comparable patchiness for a variety of components of aquatic ecosystems. Therefore, the subsamples of the original Niskin bottle samples cannot be regarded as homogeneous (Figure 1.1C), and the results of any comparison conducted between the parameters estimated from subsamples within the bottle are questionable.

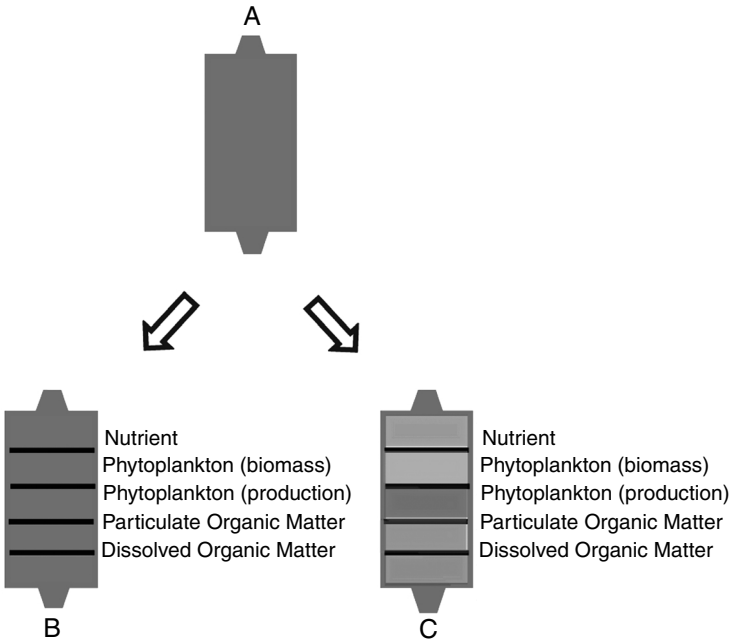


**FIGURE 1.1** Schematic illustration of a standard sampling procedure using a Niskin bottle, the elementary sampling unit in aquatic ecology (A) The study of different parameters estimated from different subsamples taken from the same bottle assumes spatial homogeneity within the sampling unit (B). However, such a sampling scheme is irrelevant if there is spatial variability within the sampling volume (C); as a result, each studied parameter is taken from a different water mass. (Adapted from Leterme, 2002.)

To investigate the impact of patchiness, we took Niskin bottle samples at two stations located in the inshore (50°47′300 N, 1°33′500 E) and the offshore (50°46′950 N, 1°16′680 E) waters of the Eastern English Channel during the spring bloom on 16 and 17 April 2002, respectively. During the recovery, the Niskin bottles were handled gently to avoid stirring of the water inside the bottles. From the 5-l bottles collected at each station, we carefully drew 192 subsamples of 20 cc. (Note: The sample analysis from a comparison experiment in which Niskin bottles collected at the same site were thoroughly stirred before drawing the subsamples is still ongoing.) The volume of the subsamples is equivalent to a vertical spatial resolution of 2.4 mm, which is comparable with the resolution of the high-resolution bio-optical sensor described in Section 1.3. After determination of chlorophyll *a* concentration following Suzuki and Ishimaru (1990), and subsequent fluorometry quantity determination (Leterme, 2002), chlorophyll *a* concentrations have been plotted against the corresponding vertical position within the Niskin bottle (Figure 1.2). The phytoplankton biomass concentrations appear clearly patchy, for both inshore and offshore waters, with very sharp variations from one sample to the next. Interestingly, the patchy vertical distribution inside the bottle is reminiscent of the profiles obtained with high-resolution sensors (cf. Section 1.3.2). The inshore chlorophyll estimates range from 0.70 to 67.03 $\mu g\ l^{-1}$ (26.68 ± 10.49; $\bar{x} \pm SD$), and a coefficient of variation CV = 39.32%. The offshore chlorophyll estimates range from 0.94 to 12.45 $\mu g\ l^{-1}$ (3.79 ± 1.88; $\bar{x} \pm SD$) and a coefficient of variation CV = 49.47%. The sharpest variations observed for the inshore and offshore samples correspond to increases in chlorophyll concentration of a factor 2.13 and 8.32 over the smallest resolution reached (i.e., 2.4 mm), respectively. This corresponds to gradients of 208 and 27.54 $\mu g\ l^{-1}\ cm^{-1}$, respectively.

The ratio between maximum and minimum chlorophyll concentrations can be considered as an estimate of phytoplankton biomass variability (Seuront and Spilmont, 2002). The ratios within the primary sampling unit are very high: 96.25 and 13.22 for inshore and offshore samples, respectively. In particular, these ratios are higher than those obtained in the framework of an annual survey conducted in the Eastern English Channel from four depths in the inshore waters and five depths in the offshore waters every 2 weeks (i.e., 30 and 6 for inshore and offshore waters, respectively; Gentilhomme and Lizon, 1998).

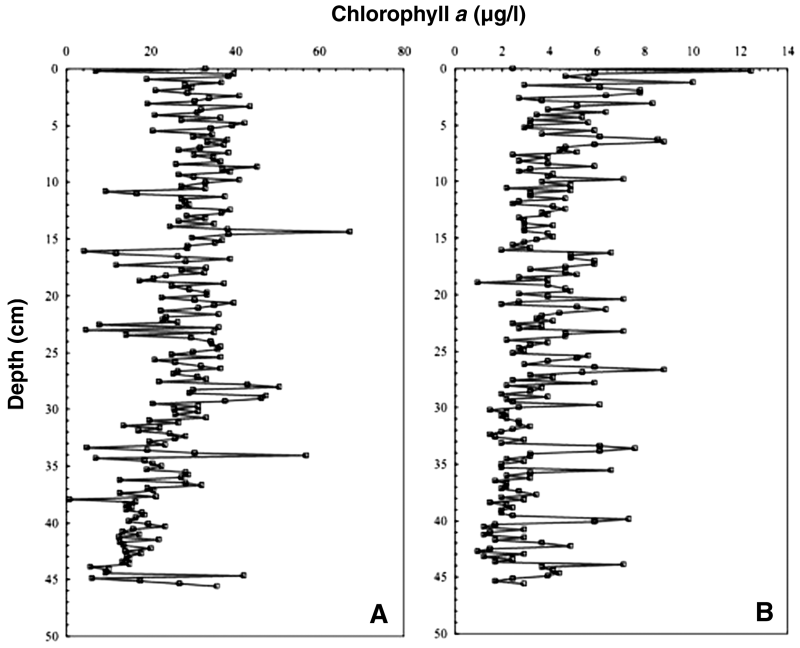


**FIGURE 1.2** Spatial distribution of chlorophyll *a* concentrations (µg $l^{-1}$) obtained from 192 subsamples of 2.4 mm vertical resolution taken from 5-l Niskin bottles, sampled in the subsurface waters at inshore (A) and offshore (B) stations located in the Eastern English Channel. (Adapted from Leterme, 2002.)

During routine fieldwork, the size of the subsamples drawn from the primary Niskin is about 15 times larger (usually 250 to 500 ml) than the subsamples drawn here. This integration averages out the small-scale variability observed in our 20-cc samples. However, Figure 1.2 shows that even under such averaging there remains a noticeable trend of the chlorophyll concentration through the Niskin bottle. This trend is more pronounced in samples collected near the sea bottom (not shown). The microscale variability within a single Niskin bottle demonstrates that small subsamples taken from a larger sample may not represent the realistic phytoplankton distribution in the ocean. As a consequence, inferring correlations (or more generally any causality) between parameters estimated from different subsamples would lead to spurious results at best, in some cases even to utterly wrong conclusions.

## 1.3 Comparison of High-Resolution Data and Conventional Techniques

A high-resolution bio-optical sensor capable of resolving centimeter scales of fluorescence and turbidity was deployed in two very different environments: Lake Biwa (Japan) and in Seto Inlet (a tidally mixed channel in Hiroshima prefecture, Japan). Fluorescence data from both deployments are presented and discussed with attention to the low-frequency response of sensor as well as the small-scale resolution. Using depth averages of the high-resolution data allows us to simulate the scale resolution of conventional sampling techniques (such as conventional field fluorometers). Structure function analysis can be used to demonstrate the qualitative and quantitative differences between the original and averaged data sets.

### 1.3.1 Instrument Description

The high-resolution sensor is mounted on the free-fall profiler "Turbulence Ocean Microstructure Acquisition Profiler" (TurboMAP). The instrument is specifically designed to record simultaneously biological and physical properties of the water column, i.e., shear, temperature, conductivity, *in vivo*

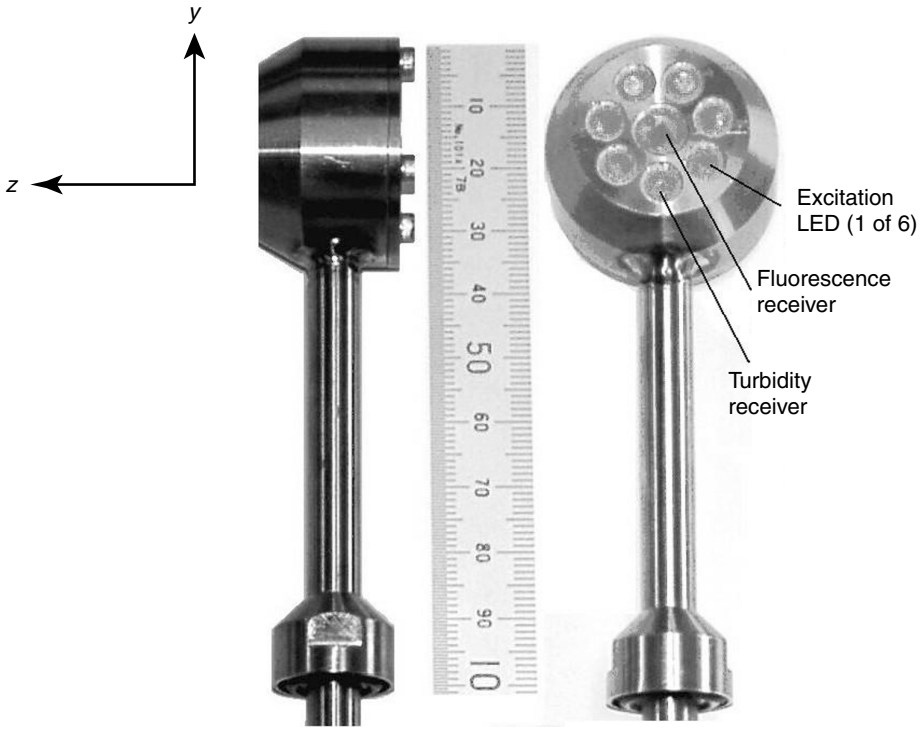


**FIGURE 1.3** Side and front view of the high-resolution bio-optical probe. Numbers on the ruler are in millimeters. During operation, the sensor travels in the *z* direction.

fluorescence, and backscatter (Wolk et al., 2002). The operating principle of the high-resolution sensor is similar to standard backscatter fluorometers; however, instead of measuring inside a small sampling cavity, the sensor projects the sampling volume away from the sensor into the free flow where the small-scale structure of the water column is not compromised by flow distortion or mixing around the sensor housing (Figure 1.3). An array of six light-emitting diodes (LEDs) provides the blue excitation light for chlorophyll *a* fluorescence (400 to 480 nm). The intersection of the light beams defines a sampling volume with a center approximately 14 mm in front of the optical receiver (640 to 720 nm). A second receiver diode detects the direct light backscatter of light from suspended particles (400 to 480 nm), which is a measure of the turbidity. Details of the sensor construction are given by Wolk et al. (2001).

The size of the sampling volume, spatial resolution, and response to naturally occurring fluorescent sources, such as algae and pure chlorophyll *a* solutions, were investigated in several laboratory tests (Wolk et al., 2001). The sampling volume is defined by the geometry of the excitation light beams and the directivity of the receiver diode. The effective size of the sampling volume was mapped by determining both the sensitivity of the probe as a function of distance from the sensor face (*z* direction) and its spatial resolution in the tangential direction (*y* direction). Figure 1.4 shows the resulting composite sensitivity. The puck centered on the origin represents the sensor head and the conical surface represents the outline of the excitation light as deduced from the LED geometry. This shape agrees with observations when the sensor is placed in turbid water. The sensitivity decreases exponentially in the *z* direction; 90% of the received fluorescent light comes from the first 25 mm in front of the sensor. Over the width of the sensor face (*x* and *y* direction) the sensitivity resembles a cosine window with a width of 20 mm.

The shape of sensor housing minimizes flow distortions and eddy generation around the sensor head. During deployment on a free-fall profiler or towed instrument, the probe looks "sideways" so that the sampling volume is located in the free-flow region. This setup preserves the small-scale structures of fluorescent material in the water column. When mounted on TurboMAP, the sensor is located on the nose cone of the instrument where there is no disturbance of the flow from other parts of the instrument.

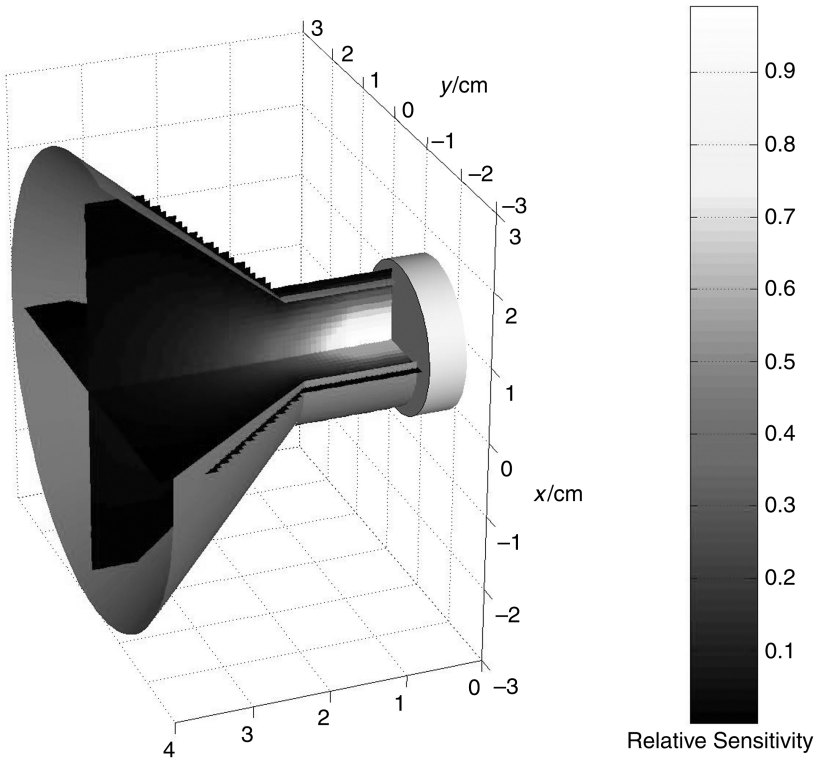


**FIGURE 1.4** Composite spatial sensitivity of the high-resolution probe deduced from laboratory experiments. The gray puck in the *x*–*y* plane represents the sensor head and the cone shows the outline of the excitation light.

### 1.3.2 Sensor Deployment

The data were collected in Lake Biwa (Figure 1.5A, B) on 31 August 2001 and in Seto Inlet (Figure 1.5C, D) on 21 August 1998. During both deployments, the small-scale sensor was mounted on the nose section of the TurboMAP profiler, which descended in free-fall mode at an average fall rate of 0.64 m $s^{-1}$ (SD = 0.01 m $s^{-1}$) in Lake Biwa and 0.69m $s^{-1}$ (SD = 0.1 m $s^{-1}$) in Seto Inlet. The TurboMAP signal is sampled at 256 Hz, which gives one data point every 2.5 mm. The signal shown is low-pass-filtered at 30 Hz to include all spatial scales resolved by the sensor while suppressing the instrumentation noise. TurboMAP reached its terminal fall speed at about 6 m depth, so both fluorescence profiles are cropped to exclude the region above 6 m.

In the Lake Biwa data, the slowly varying part of the fluorescence signal shows a well-mixed region between 6 and 9 m depth, followed by a rapid decrease between 9 and 11 m, coinciding with the temperature drop. The temperature signals are almost constant between 11 and 14 m, and the fluorescence signal also shows homogeneous features. The signal then continues to decrease slowly between 11 and 25 m, and below 25 m it is constant within the standard deviation of the signal for that depth range. The sharp "fluorocline" is ubiquitous in all profiles collected at the 4-day Lake Biwa campaign.

The dotted line in Figure 1.5B is the 1-m depth-averaged fluorometer signal, which represents the signal we would expect from a fluorometer mounted on a typical CTD cage under the same experimental conditions. Rather than descending steadily, CTD cages often heave as a result of the ship's roll. Typical CTD cages with bottle samplers have a length and width of approximately 1 m, and thus one cannot expect to obtain a scale resolution of less than 1 m from such measurement. We note, however, that under certain conditions it is possible to obtain much higher spatial resolution. Robert C. Beardsley

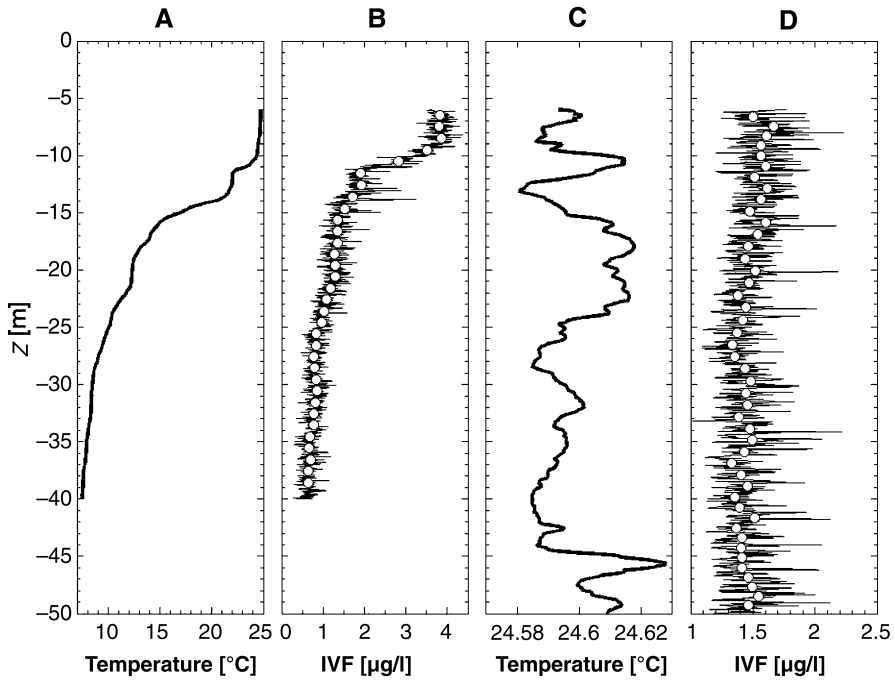


**FIGURE 1.5** Temperature and *in vivo* fluorescence measured by TurboMAP in Lake Biwa (A, B) and in Seto Inlet (C, D). The high-resolution fluorescence signal from TurboMAP (black line) and after 1-m averaging (open dots). Note that the averaged signal is similar to the profiles that could have been obtained using the conventional CTD fluorescence sensor.

(personal communication, 2003) recently obtained temperature microstructure measurements with a resolution of O ($10^{-2}$) m from CTD rosette sampler that was lowered from an icebreaker in the ice of the Antarctic. One of the Niskin bottles of the rosette was replaced with the microstructure instrument and the CTD was lowered using the ship's CTD winch.

The numerous narrow excursions (or "spikes") seen in the high-resolution signal (e.g., at $z = -13.8$, –15.0, and –16.5 m) have a typical width between 5 and 10 cm, and they are caused by small patches of algae moving relative to the sensor. The same characteristic of the fluorescence signal is also evident in the data from the Seto Inlet tidal channel, where the temperature varied only in a narrow range of 0.05°C (Figure 1.5C). Even though the water column was well mixed throughout, the fluorescence signal (Figure 1.5D) shows spikes caused by particulate or aggregate phytoplankton. Clearly, in both the Biwa and Seto data sets the rich fine structure evident in the high-resolution signal is lost in the averaged data (Figure 1.5B, D).

### 1.3.3 Differential Structure of Standard and High-Resolution Fluorescence Signals

To investigate the structure of *in vivo* fluorescence signals, we use two related but conceptually different analysis methods. The first method is based on the study of the cumulative density function (CDF), defined as:

$$P[X > x] \propto x^{-\phi} \tag{1.1}$$

where $x$ is a threshold value, and $\phi$ is the slope of a log–log plot of $P[X > x]$ vs. $x$. Note that Equation 1.1 can be equivalently rewritten in terms of the probability density function (PDF) as $P[X = x] \propto x^{-\gamma}$, where $\gamma$ ($\gamma = \phi + 1$) is the slope of a log–log plot of $P[X = x]$ vs. $x$, respectively. The absolute of the algebraic tail of the CDF is directly related to the moment of divergence $q_D$ as $q_D = \phi$, and might be a signature of a multifractal behavior (Schertzer et al., 1988). The moment of divergence characterizes the highest

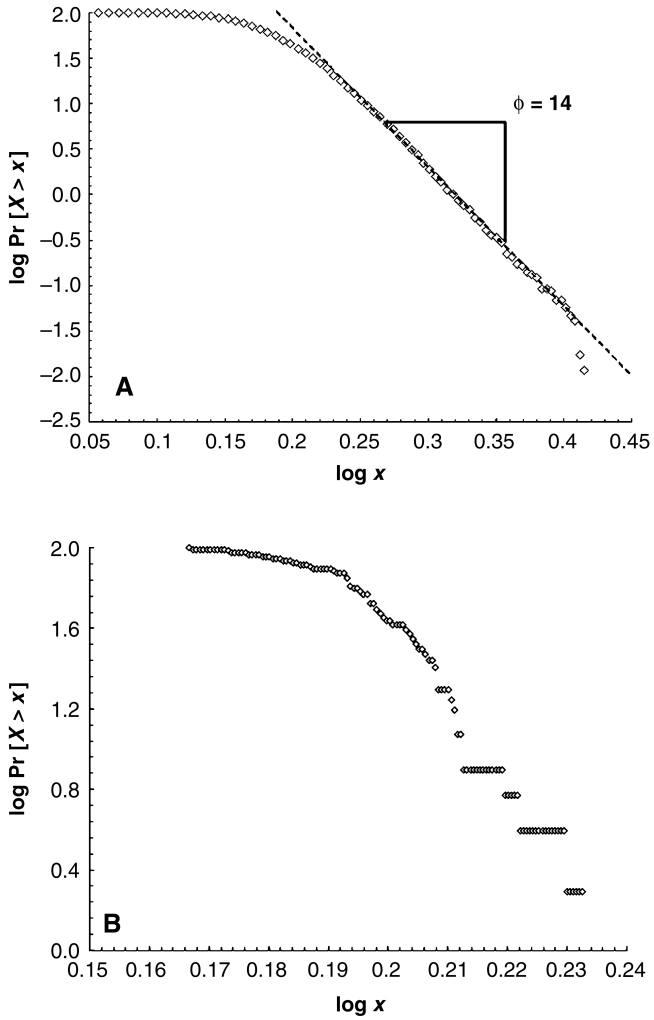


**FIGURE 1.6** The CDF $P[X > x]$ vs. $x^{-\phi}$ in a log–log plot of a high-resolution fluorescence vertical profile recorded with TurboMAP in Seto Inlet (A), compared with its 1-m resolution average (B).

statistical moment that can be reliably estimated from a given data set. For moments higher than $q_D$, the moments cannot be defined as their values becomes intrinsically linked to the length of the data sets, and thus diverge.

The CPD of the *in vivo* fluorescence profile shown in Figure 1.5D is characterized in a log–log plot by a linear behavior (Figure 1.6A) for fluorescence values bounded between 1.74 and 2.51 with a characteristic slope $\phi = 14$ ($r^2 = 0.99$), which is in the range of $\phi$ values estimated for all the vertical profiles recorded in Seto Inlet, with $\phi = 13.68 \pm 1.45$ ($\bar{x} \pm$ SD). The roll off observed for highest and lowest fluorescence values are related to systematic oversampling and undersampling of, respectively, the most common (i.e., the lowest) and most infrequent (i.e., the highest) fluorescence values. Similar results have been obtained from all the profiles recorded in Lake Biwa (not shown) with a slightly shallower slope $\phi = 11.25 \pm 1.50$ ($\bar{x} \pm$ SD). On the other hand, the CDF estimated from the 1-m resolution fluorescence profiles (Figure 1.6B) do not exhibit the specific features observed from the high-resolution profiles (Figure 1.6A). While the roll off toward high probability related to an oversampling of the most common fluorescence values is still visible, both the linear behavior and the roll off toward low probability has disappeared, demonstrating the inability of a low-resolution sampling process to capture the micro-scale structure of fluorescence distributions.

The second method of analysis is specifically designed to quantify intermittency by adopting a generalization of the $q$th-order structure functions, defined by

$$\left\langle \left(\Delta IVF_l\right)^q \right\rangle \propto l^{\zeta(q)} \tag{1.2}$$

where $\Delta IVF_l$ is the fluctuation of the *in vivo* fluorescence signal at scale $l$ and angle brackets indicating an average; see Seuront et al. (1999; Chapter 22, this volume). Equation 1.2 thus gives the scale-invariant structure function exponents $\zeta(q)$, which characterize the statistics of the whole field. The scaling exponent $\zeta(q)$ is estimated from the slope of the linear trend of $\left\langle \left(\Delta IVF_l\right)^q \right\rangle$ vs. $l$ in a log–log plot, for different values of the statistical order of moments $q$. For example, the first moment ($q = 1$) gives the constant scaling exponent $\zeta(1) = H$, which describes the scale dependence of the average fluctuations. When $H \neq 1$ the fluctuations $\Delta IVF_l$ will depend on the spatial scale; $H$ then characterizes the degree of stationarity of the process. The second moment ($q = 2$) is linked to the slope $\beta = 1 + \zeta(2)$ of the signal's power spectrum. For fractal processes, the scaling exponent $\zeta(q)$ is linear and is defined as $\zeta(q) = qH$. In particular, $\zeta(q) = q/2$ for a Brownian process and $\zeta(q) = q/3$ for nonintermittent, homogeneous turbulence. On the other hand, $\zeta(q)$ is a nonlinear convex function for multifractal (i.e., intermittent) processes.

The structure functions $\left\langle \left(\Delta IVF_l\right)^q \right\rangle$ of the high-resolution TurboMAP profiles from Lake Biwa for $q = 1,2$, and 3 are shown in Figure 1.7. The structure function scaling exponents $\zeta(q)$ were determined following Seuront and Lagadeuc (1997) by linear regression of $\log\left\langle \left(\Delta IVF_l\right)^q \right\rangle$ vs. $\log l$ over the range of scales that maximized the coefficient of determination $r^2$ and minimized the total sum of squared residuals for the regression. For spatial scales larger than 1 m, high-resolution and low-resolution structure functions are similar, as is seen from the identical slopes at these scales (Figure 1.8). However, the high-resolution structure functions clearly exhibit a scaling range for spatial scales bounded between 0.015 and 0.113 m for Lake Biwa (closed symbols; Figure 1.7) and between 0.050 and 0.333 m for Seto Inlet. For these two scaling ranges, the empirical exponents $\zeta(q)$ were computed for $q$ between 0 and 5 with increments of 0.1. The resulting empirical curves (diamond symbols in Figure 1.8) are clearly nonlinear, showing that the fluorescence fluctuations for $0.015 \leq l \leq 0.113$ m in Lake Biwa and $0.050 \leq l \leq 0.333$ m in Seto Inlet can be regarded as multifractal. The TurboMAP curve clearly deviates from the straight, dotted line expected for nonintermittent turbulence ($\beta = 5/3$). In particular, the scaling of the first moment gives $H = \zeta(1) = 0.34 \pm 0.01$ (the error bars result from the separate analysis of different sections of the vertical profile). This indicates that the fluorescence distribution is far from conservative or stationary (in which case $H = 0$). The scaling of the second-order moment confirms the estimate from the slope $\beta = 1 + \zeta(2)$ of the power spectrum of the high-resolution fluorescence profile (not shown): $\zeta(2) = 0.64 \pm 0.02$, consistent within their 95% confidence intervals.

## 1.4 Conclusion

Data sets of biological parameters collected with conventional sampling methods were compared to records of a recently developed high-resolution fluorometer. It was shown that the conventional procedures can lead to a misrepresentation of the structure of the aquatic system. A random sample drawn from a Niskin bottle, for example, can give an erroneous representation of the average concentration of chlorophyll *a* concentration at the depth where the bottle sample was taken. Variations inside the bottle exceeded the annual variations of chlorophyll *a* at the sampling site.

The low-resolution fluorescence data, which are similar to what could be obtained from a CTD-mounted *in situ* fluorometer, showed a markedly different structure from the high-resolution data. Although the shape (i.e., slow variation) of the measured fluorescence signal (i.e., CTD-like sensor) is similar to many other fluorescence profiles published in the literature, the high-frequency part of the data shows structures that are not readily accessible with conventional instrumentation.

The importance of obtaining high-resolution biological records to our understanding of the aquatic ecosystem is undisputed. It was shown how the use of multifractal analysis gives us the necessary tools to condense the high-resolution data efficiently, which allows us to describe quantitatively the nature

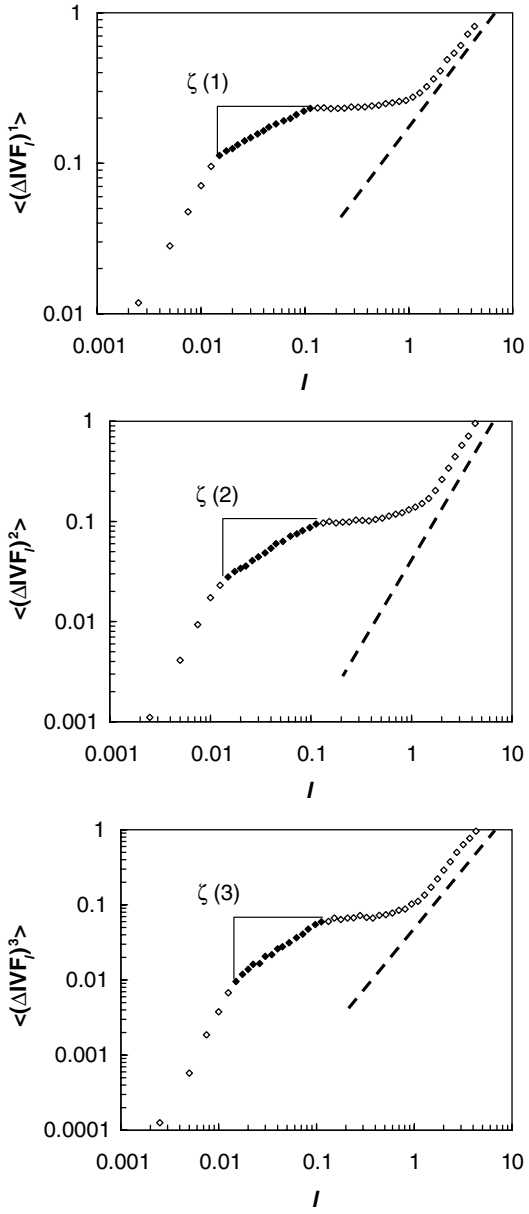


**FIGURE 1.7** The structure functions $\left\langle \left(\Delta IVF_l\right)^q \right\rangle$ vs. $l$ in log–log plots for $q$ = 1, 2, and 3 (from top to bottom) for the TurboMAP fluorescence profile. The slopes of the closed symbols provide estimates of the first, second, and third scaling exponents $\zeta(1) = H$, $\zeta(2)$, and $\zeta(3)$. The dashed lines correspond to the slopes of the structure functions obtained from the 1-m resolution fluorescence profile.

(e.g., degree of intermittency) of the distributions. We now have at our disposal the instrumentation and data processing tools necessary for a systematic investigation of the smallest scales of aquatic ecology.

## Acknowledgments

The field campaign at Lake Biwa was supported by a grant from Lake Biwa Research Institute. Daniel Kamykowski provided useful comments on an early version of this chapter.

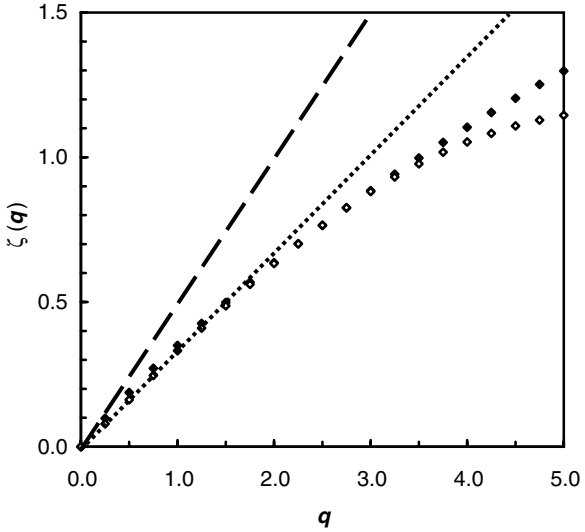


**FIGURE 1.8** The empirical scaling exponents $\zeta(q)$ obtained from the TurboMAP fluorescence profile in Lake Biwa (open diamonds) and in Seto Inlet (black diamonds). The nonlinear behavior is the signature of the multifractal character of the fluorescence fluctuations. The functions for a Brownian motion process (dashed line) and for nonintermittent turbulence (dotted line) are shown for comparison.

## References

Cowles, T.J., R.A. Desiderio, and M.-E. Carr, 1998: Small-scale planktonic structure: persistence and trophic consequences. *Oceanography,* 11(1), 4–9.

Denman, K.L. and T.M. Powell, 1984: Effects of physical processes on planktonic ecosystems in the coastal ocean. *Oceanogr. Mar. Biol. Annu. Rev.*, 22, 125–168.

Desiderio, R.A., T.J. Cowles, and J.N. Moum, 1993: Microstructure profiles of laser-induced chlorophyll fluorescence spectra: evaluation of backscatter and forward-scatter fiber-optic sensors. *J. Atmos. Ocean. Tech.*, 10, 209–224.

Donaghay, P., H.M. Rines, and J.M. Sieburth, 1992: Simultaneous sampling of fine scale biological, chemical, and physical structure in stratified waters. *Arch. Hydrobiol. Beih.*, 36, 97–108.

Franks, P.J.S. and J.F. Jaffe, 2001: Microscale distributions of phytoplankton: initial results from a two-dimensional imaging fluorometer, OSST. *Mar. Ecol. Prog. Ser.*, 220, 59–72.

Gentilhomme, V. and F. Lizon, 1998: Seasonal cycle of nitrogen and phytoplankton biomass in a well-mixed coastal system (Eastern English Channel). *Hydrobiologia*, 361, 191–199.

Hanson, A.K. and P.L. Donaghay, 1998: Micro- to fine-scale chemical gradients and layers in stratified coastal waters. *Oceanography*, 11, 10–17.

Holliday, D.V., R.E. Pieper, C.F. Greenlaw, and J.K. Dawson, 1998: Acoustical sensing of small-scale vertical structures in zooplankton assemblages. *Oceanography*, 11, 18–23.

Hutchinson, G.E., 1961: The paradox of the plankton. *Am. Nat.*, 95, 137–145.

Jackson, G.A. and A. Burd, 1998: Aggregation in the marine environment. *Environ. Sci. Tech.*, 32, 2805–2814.

Jaffe, J.F., P.J.S. Franks, and A.W. Leising, 1998: Simultaneous imaging of phytoplankton and zooplankton distributions. *Oceanography*, 11, 24–29.

Leterme, S., 2002: Microscale Variability of Phytoplankton Biomass in Turbulent Environment. Diplôme Supérieur de Recherche thesis, Université des Sciences et Technologies de Lille, France.

Mackas D.L., K.L. Denman, and M.R. Abbott, 1985: Plankton patchiness: biology in the physical vernacular. *Bull. Mar. Sci.*, 37, 652–674.

Mitchell J.G. and J.A. Fuhrman, 1989: Centimeter scale vertical heterogeneity in bacteria and chlorophyll *a. Mar. Ecol. Prog. Ser.,* 54, 141–148.

Pascual, M., F.A. Ascioti, and H. Caswell, 1995: Intermittency in the plankton: a multifractal analysis of zooplankton biomass variability. *J. Plankton Res.*, 17, 1209–1232.

Petrenko, A.A., J.R.V. Zaneveld, W.S. Pegau, A.H. Barnard, and C.D. Mobley, 1998: Effects of a thin layer on reflectance and remote-sensing reflectance. *Oceanography*, 11, 48–50.

Platt, T., W.G. Harrison, M.R. Lewis, W.K.W. Li, S. Sathyendranath, R.E. Smith, and A.F. Vezina, 1989: Biological production in the oceans: the case for a consensus. *Mar. Ecol. Prog. Ser.*, 52, 77–88.

Scheffer, M., 1995: Implications of spatial heterogeneity for the paradox of enrichment. *Ecology*, 76, 2270–2277.

Schertzer, D., S. Lovejoy, F. Schmitt, Y. Chigirinskaya, and D. Marsan, 1998: Multifractal cascade dynamics and turbulent intermittency. *Fractals*, 5, 427–471.

Schmitt, F. and L. Seuront, 2001: Multifractal random walk in copepod behavior. *Physica A*, 301, 375–396.

Seuront, L., 2001: Microscale processes in the ocean: why are they so important for ecosystem functioning? *La Mer*, 39, 1–8.

Seuront, L. and Y. Lagadeuc, 1997: Characterisation of space–time variability in stratified and mixed coastal waters (Baie des Chaleurs, Québec, Canada): application of fractal theory. *Mar. Ecol. Prog. Ser.*, 159, 81–95.

Seuront, L. and N. Spilmont, 2002: Self-organized criticality in intertidal microphytobenthos patch patterns. *Physica A*, 313, 513–539.

Seuront, L., F. Schmitt, Y. Lagadeuc, D. Schertzer, and S. Lovejoy, 1999: Universal multifractal analysis as a tool to characterize multiscale intermittent patterns: example of phytoplankton distribution in turbulent coastal waters. *J. Plankton Res.*, 21, 877–922.

Seuront, L., F. Schmitt, and Y. Lagadeuc, 2001: Turbulence intermittency, small-scale phytoplankton patchiness and encounter rates in plankton: where do we go from here? *Deep-Sea Res. I*, 48, 1199–1215.

Seuront, L., V. Gentilhomme, and Y. Lagadeuc, 2002: Small-scale nutrient patches in tidally mixed coastal waters. *Mar. Ecol. Prog. Ser.*, 232, 29–44.

Seymour, J., J.G. Mitchell, L. Pearson, and R.L. Waters, 2000: Heterogeneity in bacterioplankton abundance at centimetre scales. *Aquat. Microbial Ecol.*, 22, 143–153.

Siegel, D.A., 1998: Resource competition in a discrete environment: why are plankton distribution paradoxical? *Limnol. Oceanogr.*, 43, 1133–1146.

Sosik, H.M. and B.G. Mitchell, 1995: Light absorption by phytoplankton, photosynthetic pigments and detritus in the California Current System. *Deep Sea Res.*, 42, 1717–1748.

Strutton, P.G., J.G. Mitchell, and J.S. Parslow, 1996: Non-linear analysis of chlorophyll *a* transects as a method of quantifying spatial structure. *J. Plankton Res.*, 18, 1717–1726.

Strutton, P.G., J.G. Mitchell, and J.S. Parslow, 1997: Using non-linear analysis to compare the spatial structure of chlorophyll with passive tracers. *J. Plankton Res.*, 19, 1553–1564.

Suzuki, R. and T. Ishimaru, 1990: An improved method for the determination of phytoplankton chlorophyll using *N*,*N*-dimethylformamide. *J. Oceanogr. Soc. Jpn.*, 46, 190–194.

Wolk, F., L. Seuront, and H. Yamazaki, 2001: Spatial resolution of a new micro-optical probe for chlorophyll and turbidity, *J. Tokyo Univ. Fish.*, 87, 13–21. (Available through the Tokyo University of Fisheries, 4-5-7 Konan, Minato-Ku, 108-8477, Tokyo, Japan.)

Wolk, F., H. Yamazaki, L. Seuront, and R.G. Lueck, 2002: A new free-fall profiler for measuring biophysical microstructure. *J. Atmos. Oceanic Technol.*, 19, 780–793.

Yamazaki, H. and T.R. Osborn, 1988: Review of oceanic turbulence: implications for biodynamics, in Rothschild, B.J., Ed., *Toward a Theory on Biological-Physical Interactions in the World Ocean*. Kluwer, Dordrecht.

Yamazaki, H. and K.D. Squires, 1996: Comparison of oceanic turbulence and copepod swimming. *Mar. Ecol. Prog. Ser.*, 144, 299–301.

Yamazaki, H., J.G. Mitchell, L. Seuront, F. Wolk, H. Li, J.R. Seymour, and R.L. Waters, 2002a: Microscale patchiness and intermittency for phytoplankton in a turbulent ocean. *Nature*, submitted.

Yamazaki, H., D.L. Mackas, and K.L. Denman, 2002b: Coupling small-scale turbulent processes with biology, in *The Sea,* A.R. Robinson, J.J. McCarthy, and B.J. Rothschild, Eds., *Biological–Physical Interactions in the Ocean,* Vol. 12. John Wiley & Sons, New York, 51–112.

Zaneveld, R.J. and W.S. Pegau, 1998: A model for the reflectance of thin layers, fronts, and internal waves and its inversion. *Oceanography*, 11, 44–47.